Cole-Puli International Conference Publishing Group

Science, Engineering and Technology Proceedings

Article

2025 International Conference on Natural Sciences, Agricultural Economics, Biomedicine and Sustainable Development (AEBSD 2025)

Terahertz Perfect Absorption Based on Ultrathin Conductive Films

KeLiang Luo [1,*]

[1] Faculty of computer science and information technology, Putra University of Malaysia, Kuala Lumpur, 43400, Malaysia

* Correspondence: KeLiang Luo, Faculty of computer science and information technology, Putra University of Malaysia, Kuala Lumpur, 43400, Malaysia

Abstract: Electromagnetic absorption is one of the most fundamental forms of light-matter interaction, spanning a broad spectral range from radio frequency to the ultraviolet band. In the terahertz (THz) regime, however, conventional materials typically exhibit weak absorption, which limits the performance of high-efficiency THz devices such as detectors, modulators, and sensors. The development of ultrathin conductive films (UTCFs), especially two-dimensional materials, offers new opportunities for enhancing THz absorption due to their unique optical and electrical characteristics. Yet, the extremely small thickness of these UTCFs often restricts their ability to sustain strong interaction with incident THz waves, making additional strategies necessary to achieve substantial absorption. In this work, using graphene as a representative UTCF, we demonstrate that near-perfect THz absorption can be realized through a total internal reflection (TIR) configuration. When the refractive index of the superstrate exceeds that of the substrate, TIR occurs once the incident angle surpasses the critical angle, enabling the confined evanescent field to interact strongly with the ultrathin film. This mechanism leads to highly efficient THz absorption in UTCF-based structures and supports a broadband and wide-angle near-perfect absorption region around the optimal absorption point. A detailed parameter-dependence analysis is conducted for both the UTCF and the surrounding dielectric environment, illustrating how the absorption peak evolves with material conductivity, film thickness, refractive-index contrast, and incidence angle. The findings provide a refined physical understanding and a practical design pathway for developing strong THz absorbers based on ultrathin conductive materials, contributing to future applications in THz sensing, imaging, and integrated photonic systems.

Keywords: perfect absorption; terahertz; ultrathin conductive films; total internal reflection

Received: 01 November 2025
Revised: 30 November 2025
Accepted: 17 December 2025
Published: 20 December 2025

1. Introduction

1.1. Background and Significance of Terahertz Technologies

Over the past few decades, the terahertz (THz) frequency band has attracted increasing attention across a wide range of scientific and engineering fields, including basic physical research and emerging industrial applications [1]. The inherent properties of THz waves-such as low photon energy, strong penetrability for many non-conductive materials, and unique spectral signatures of numerous molecules-have facilitated the rapid development of THz-based technologies. These capabilities have enabled progress in advanced information and communications systems, biomedical imaging, fingerprint spectroscopy, nondestructive testing, and security inspection, demonstrating the strategic

importance of THz science in modern technological innovation [2,3]. As these applications mature, the demand for compact, efficient, and robust THz functional components continues to grow, driving researchers to explore new approaches for enhancing THz-matter interactions.

Despite these promising developments, light-matter interaction in the THz regime generally remains weak. The limited availability of materials with strong THz responses, combined with the challenges of fabricating complex THz structures, often results in insufficient absorption efficiency. These limitations constrain the design of high-performance THz devices such as modulators, detectors, sensors, and absorbers. Consequently, the development of materials and mechanisms capable of significantly enhancing THz absorption has become an essential research direction [4,5].

To meet these demands, researchers have sought material platforms with intrinsic flexibility, high tunability, and strong interaction with electromagnetic waves. In particular, low-dimensional and ultrathin conductive materials have gradually emerged as promising candidates due to their unique optical responses and compatibility with advanced photonic designs. These advantages make them suitable for practical THz devices intended for sensing, wave manipulation, imaging, and energy harvesting.

1.2. Advances in Low-Dimensional THz Absorbers

Recent progress in low-dimensional materials has provided new opportunities for enhancing the interaction between THz waves and ultrathin structures [6]. Many types of THz absorbers have been proposed, particularly those relying on thin-film materials to create compact, tunable, and highly efficient device architectures [7]. For example, the use of graphene in THz absorbers has demonstrated that broadband absorption can be achieved by carefully tailoring the impedance of the structure, enabling absorption levels around 50% within the 0.2-1.2 THz range under impedance-matching conditions [8]. Such designs highlight the potential of two-dimensional materials to support enhanced THz responses compared with conventional bulk materials.

Beyond graphene, ultrathin MXene-based films have also been identified as promising THz absorbers, achieving broadband absorption over the 0.5-10 THz range [9]. The primary operating principle of these absorbers is the impedance-matching mechanism, where the sheet resistance of the ultrathin conductive film (UTCF) approaches half of the free-space characteristic impedance (Z_0 = 377 Ω). Under these conditions, the maximum coupling between the incident THz wave and the suspended UTCF occurs, leading to absorption values approaching 50% [10,11]. Although this represents a significant enhancement for extremely thin films, it remains insufficient for applications requiring strong or near-perfect absorption [12-14].

These developments reveal a clear challenge: while low-dimensional UTCFs can interact effectively with THz waves, their thickness is often too small to sustain the level of interaction needed for high absorption. This motivates the search for novel mechanisms that can amplify the field intensity around such ultrathin materials, enabling absorption levels beyond the intrinsic 50% limit of impedance matching.

1.3. Motivation and Contribution of This Work

To address these challenges, this work proposes a new approach for realizing strong THz absorption through a simple and physically intuitive configuration combining UTCFs with a total internal reflection (TIR) structure. In this design, perfect absorption (PA) is achieved when the incident angle exceeds the critical angle at which TIR occurs, resulting in a confined evanescent field that strongly interacts with the ultrathin film. This mechanism effectively bypasses the intrinsic absorption limitations of freestanding UTCFs and enables significantly enhanced interaction between the THz field and the conductive layer.

Without loss of generality, graphene is chosen as the representative UTCF to demonstrate the feasibility and performance of the proposed TIR-based THz perfect absorber. By exploiting the strong evanescent field generated under TIR conditions, the structure supports both near-perfect and wide-angle absorption around the PA point, providing superior performance compared with conventional thin-film absorbers. Moreover, the concept requires only a simple dielectric-graphene-substrate configuration, making it more practical and easier to fabricate than many existing metamaterial-based absorbers.

In addition, a comprehensive parameter analysis is conducted to systematically investigate the absorption characteristics of the proposed THz structure. The study examines the influence of graphene conductivity, film thickness (or equivalently sheet resistance), refractive-index contrast between the substrate and superstrate, and incident angle. The evolution of the PA point is clearly revealed through these analyses, enabling deeper physical understanding and offering useful guidelines for designing future THz absorbers based on ultrathin materials. The proposed approach thus provides a promising design pathway for high-performance THz components and paves the way for practical applications in sensing, imaging, detection, and integrated THz photonics.

2. Methods

2.1. Structural Configuration of the UTCF-Based THz Absorber

The terahertz perfect absorber investigated in this work is constructed using a simple trilayer configuration composed of a dielectric superstrate, an ultrathin conductive film (UTCF), and a dielectric substrate. The overall structure is illustrated in Figure 1 (in Section 3), where the UTCF is embedded at the interface between the two dielectrics. The superstrate and substrate are modeled as nonmagnetic, lossless media with relative permittivities ε_1 and ε_2 (or equivalently refractive indices n_1 and n_2). These parameters are defined as $\varepsilon_1 = n_1^2$ and $\varepsilon_2 = n_2^2$, and they remain constant throughout the terahertz frequency range considered.

The UTCF is represented as an infinitesimally thin conductive boundary characterized by a sheet conductivity $\sigma(\omega)$. This conductivity is both complex-valued and frequency-dependent, making it suitable for describing the dynamical response of low-dimensional materials at terahertz frequencies. An obliquely incident plane wave with incident angle θ is directed from the superstrate toward the UTCF, and depending on the refractive-index contrast ($n_1 > n_2$), total internal reflection (TIR) may occur when θ is larger than the critical angle $\theta\_c = \arcsin(n_2/n_1)$. Under this condition, the evanescent field localized at the interface interacts strongly with the UTCF, enabling the emergence of perfect absorption (PA).

This structural model allows the absorber to be described analytically using classical electromagnetic theory, while avoiding the need for patterned metasurfaces or complex multilayer architectures. All physical phenomena observed in the results arise from the interplay between the UTCF conductivity, the refractive-index contrast, and the evanescent field generated in the TIR regime.

2.2. Electromagnetic Framework and Calculation Procedure

The optical response of the structure-including transmission, reflection, and absorption-is calculated by solving Maxwell's equations with appropriate boundary conditions at the interface containing the UTCF. The system is treated as a one-dimensional multilayer problem with an ultrathin conductive boundary. Because the UTCF thickness is negligible compared to the incident wavelength, the film is incorporated through a surface current density $J\_s = \sigma E\_t$, where E_t is the tangential electric field at the interface.

The Fresnel coefficients for p- and s-polarizations are modified to include the sheet conductivity term, yielding expressions of the form:

1) Reflection coefficient: $R = |r(\omega, \theta)|^2$
2) Transmission coefficient: $T = |t(\omega, \theta)|^2$
3) Absorption: $A = 1 - R - T$

When $\theta > \theta_c$, the transmission T becomes zero due to TIR, simplifying the absorption condition to $A = 1 - R$. Therefore, perfect absorption is achieved when the reflection coefficient satisfies $r(\omega, \theta) = 0$.

Numerical evaluations of R, T, and A are performed over a two-dimensional parameter space spanned by frequency and incident angle. This allows visualization of PA points and broadband absorption regions. The method provides a direct and intuitive way to analyze the conditions required for achieving PA, including impedance matching and evanescent-field enhancement.

2.3. Material Model for Graphene and Parameter Definitions

To describe the electromagnetic behavior of the UTCF, graphene is selected because it naturally exhibits tunable terahertz conductivity and is widely implemented in compact THz devices. When the photon energy $\hbar\omega$ is much lower than the graphene Fermi level E_F, interband transitions can be neglected. In this regime, the conductivity is dominated by intraband (free-carrier) processes and is accurately captured by the Drude-like model:

$$\sigma(\omega) = (e^2 E_F) / (\pi\hbar^2 (\gamma - i\omega)) \quad (1)$$

where ω is the angular frequency, γ is the scattering rate, e is the electron charge, and $\hbar$ is the reduced Planck constant.

To further quantify the carrier scattering, a scattering energy is introduced as:

$$\Gamma = \hbar\gamma \quad (2)$$

The model parameters used in this study-such as E_F and Γ-are selected to represent realistic graphene conditions under typical doping and room-temperature environments. The frequency-dependent real and imaginary parts of $\sigma(\omega)$ (shown in Figure 2 in Section 3) reveal the dominance of the free-carrier response in the THz range, demonstrating their role in determining the impedance-matching condition and the resulting PA behavior.

2.4. Parameter Scanning and Numerical Analysis

To fully understand the absorption characteristics of the proposed THz PA system, systematic parameter sweeps are performed. These include variations in:

1) Fermi level E_F, representing tunable carrier concentration
2) Scattering energy Γ, representing carrier mobility and disorder
3) Superstrate permittivity ε_1, determining the onset of TIR
4) Incident angle θ, determining the evanescent-field strength
5) Frequency f, covering the full THz range of interest

Each parameter sweep produces a two-dimensional absorption map that reveals conditions for PA, broadband absorption, or reduced interaction. This approach enables identification of multiple PA points, the evolution of absorption bands, the sensitivity of PA to material losses, and the role of refractive-index contrast in supporting or suppressing TIR.

Together, these methods form a coherent and comprehensive analytical framework, allowing both physical interpretation and design optimization of UTCF-based THz perfect absorbers.

3. Results and Discussion

3.1. Structure and Model

The basic structure of the UTCF-based THz perfect absorber is shown in Figure. 1. The UTCF is located at the interface between the supersubstrate and the substrate. The permittivities (refractive indices) of the supersubstrate and the substrate are indicated by two real constants ε_1 and ε_2 (n_1 and n_2), where $\varepsilon_1 = n_1^2$ and $\varepsilon_2 = n_2^2$. The conductance of the

UTCF is σ, which is usually complex and frequency-dependent. The THz wave is incident on the UTCF at an oblique angle θ.

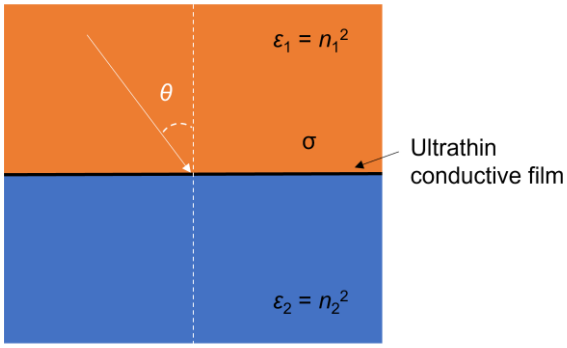

Figure 1. | Schematic picture for THz PA based on ultrathin conductive films.

For the UTCF, the graphene is selected because of its tunable electronic and optical properties, which are widely used in related studies of integrated THz devices. When the photon energy of the incident wave is much lower than the Fermi level of graphene, the interband contribution to the graphene optical conductivity is negligible. Therefore, for frequencies in the THz and mid-IR spectral range, at room temperature, when the graphene is under typical doping levels, the complexed and frequency-dependent conductivity of graphene can be described by the Drude-like formula,

$$\sigma(\omega) = i\frac{e^2}{\pi\hbar^2}\frac{E_F}{\omega+i\gamma} \quad (3)$$

where ω is the angular frequency of the incident THz wave, E_F is the Fermi level of the graphene, and γ is the scattering rate. e is the electron charge, and $\hbar$ is the reduced Planck's constant. The corresponding scattering energy can be characterized by

$$\Gamma = \hbar\gamma \quad (4)$$

Here, the E_F and Γ of graphene are set as 0.5 eV and 5 meV, respectively. The real and imaginary parts of graphene THz conductivity are summarized in Figure. 2. In this frequency range, free-carrier response dominates, indicating direct information about the Dirac fermion electrical transport [15,16].

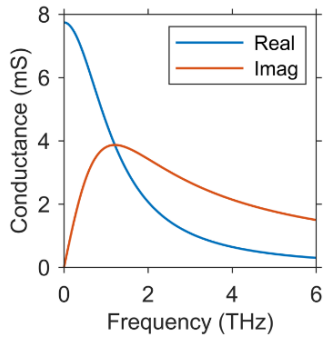

Figure 2. | Real and imaginary parts of the graphene THz conductivity.

3.2. Terahertz Perfect Absorption

As shown in Figure. 3, the transmission, reflection, and absorption of the graphene-based THz perfect absorber are calculated via electromagnetic theory. The permittivities of the superstrate and substrate are set to $\varepsilon_1 = 4$ and $\varepsilon_2 = 1$. When the incident angle is higher than the critical angle ($\arcsin(n_2/n_1) = 30°$ here) of the system, TIR occurs, and the

transmission is completely suppressed (Figure. 3a). Therefore, the THz PA can be achieved when the reflection equals zero.

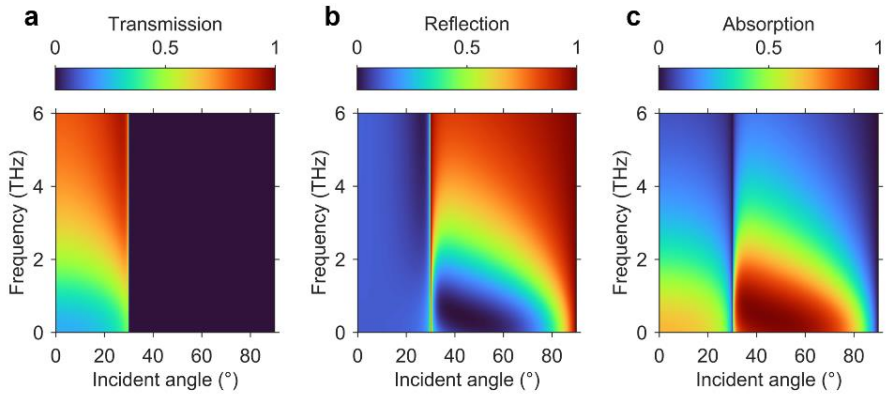

Figure 3. | Transmission, reflection, and absorption of the graphene-based THz perfect absorber.

As shown in Figure. 3b, the reflection is completely suppressed in the low-frequency range (0-1 THz) in certain incident angles, which corresponds to the THz PA (Figure. 3c). From Figure. 3c, it can be observed that strong THz absorption exists in a relatively broad range of frequency and incident angle, indicating the robustness of the strong THz absorption in UTCF-based THz absorbers.

3.3. Dependence on Thin-Film Parameters

Further, the parameter dependence of the UTCF is conducted for the understanding of this THz PA. As shown in Figure. 4, the dependence on the Fermi level of graphene is calculated, which is selected as E_F = 0.3 eV, 0.7 eV, and 1.0 eV. Γ = 0.5 meV is fixed.

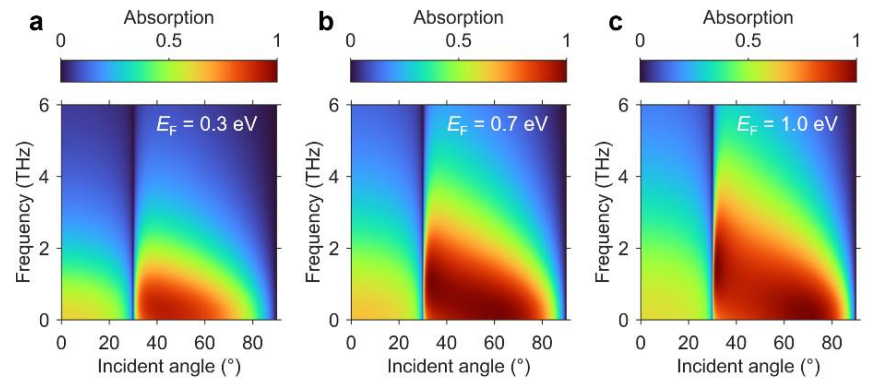

Figure 4. | Dependence of the Fermi level of the graphene.

When E_F = 0.3 eV, the THz PA disappears for any frequency and incident angle because the THz conductivity of the graphene can not satisfy the impedance-matched condition. However, similar to the result shown in Figure. 3c, the THz PA appears again when E_F = 0.7 eV. Interestingly, it seems to have two THz PA points in the considered two-dimensional (2D) plane spanned by the frequency and incident angle, where the first one is located near the critical angle and the second one is situated at larger angles. From Figure. 4, it can also be found that the frequency of THz PA increases with the enlarged E_F.

The results in Figure. 4 demonstrate that the THz PA can be achieved in a simple configuration with only a single conductive interface. Besides, the impedance-matched condition is required for the THz PA, where two THz PA points could be possible in a high-enough E_F.

Next, the dependence of the carrier scattering effects is considered in Figure. 5, where Γ = 3 meV, 8 meV, and 12 meV are selected for the calculation, and E_F = 0.5 eV is fixed. As shown in Figure. 5, with the increase of Γ, the maximum THz absorption in the considered 2D plane declines gradually, and the THz PA disappears. Besides, the region of high THz absorption extends to higher frequencies and lower incident angles. These properties are opposite to the effect of E_F (Figure. 4) because the increased Γ would suppress the THz conductivity of the UTCF. Despite that, the THz absorption in the UTCF is strong (>50%) in a broad range, even when the carrier scattering effects are intense. Compared to the results of Figure. 5a and Figure. 3c, it can be observed that two THz PA points can also be supported when the carrier scattering effects are decreased.

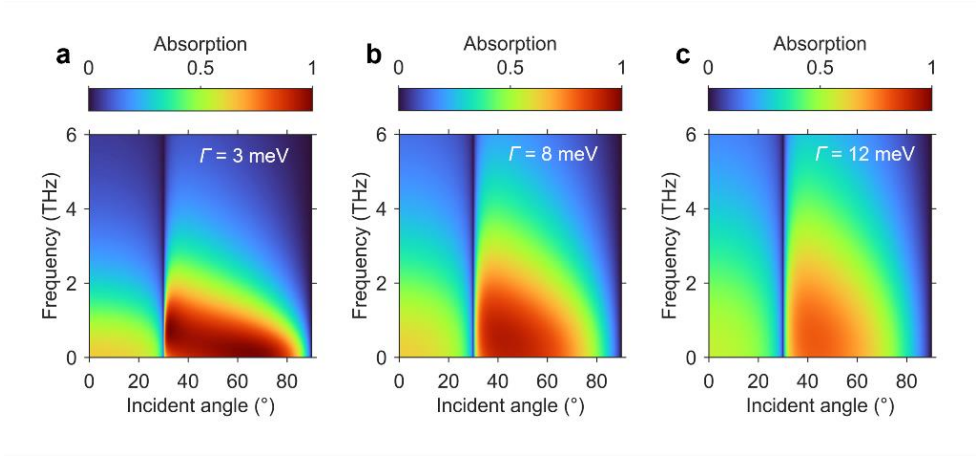

Figure 5. | Dependence of the scattering rate of the graphene.

To conclude, the results in Figure. 4 and Figure. 5 demonstrate that the properties of THz PA are highly tunable and controllable by tuning the graphene parameters.

3.4. Dependence on Superstrate Refractive Indices

Finally, the influences of the superstrate are analyzed in Figure. 6, where ε_1 = 9, 2, 1 are selected for calculation. When ε_1 is changed, the critical angle is also modified. Specifically, when ε_1 declines, the critical angle increases. Compared to the results of Figure. 6a (ε_1 = 9), Figure. 3c (ε_1 = 4), and Figure. 6b (ε_1 = 2), it can be observed that the THz PA exists in all three cases, where the THz PA points are located in the low-frequency range when the condition for the TIR is satisfied.

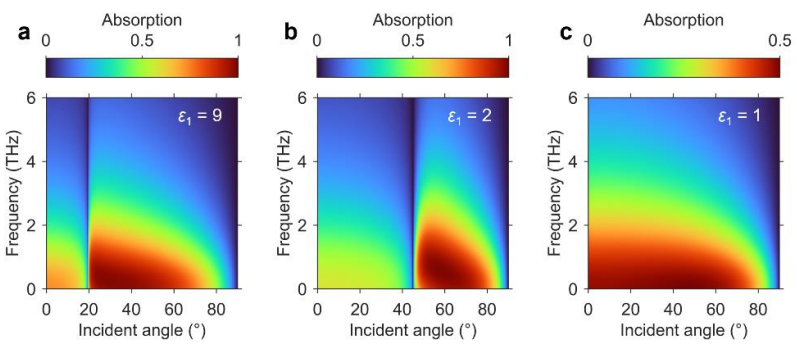

Figure 6. | Dependence of the refractive index of the superstrate.

However, as shown in Figure. 6c, when ε_1 = 1, the THz PA can not be supported because the condition for the TIR is broken, where the maximum THz absorption is up to 50% when the THz conductivity of the UTCF is impedance-matched.

The results in Figure. 6 prove that the UTCF-based THz PA proposed in this work depends on the permittivity or refractive index of the superstrate and substrate, which should be considered by combining the impedance-matched condition to ensure the TIR is achievable.

4. Conclusions

In this work, a novel THz PA based on the UTCF is proposed and demonstrated, where the configuration is simple to realize easily via a TIR structure. The conditions and properties of the UTCF-based THz PA are analyzed and discussed in detail. The ideas and results used in this work can also be extended to a broader materials and structures based on various UTCFs.

References

1. M. Tonouchi, "Cutting-edge terahertz technology," *Nature photonics*, vol. 1, no. 2, pp. 97-105, 2007. doi: 10.1038/nphoton.2007.3
2. S. S. Dhillon, M. S. Vitiello, E. H. Linfield, A. G. Davies, M. C. Hoffmann, J. Booske, and M. B. Johnston, "The 2017 terahertz science and technology roadmap," *Journal of Physics D: Applied Physics*, vol. 50, no. 4, p. 043001, 2017. doi: 10.1088/1361-6463/50/4/043001
3. A. Leitenstorfer, A. S. Moskalenko, T. Kampfrath, J. Kono, E. Castro-Camus, K. Peng, and J. Cunningham, "The 2023 terahertz science and technology roadmap," *Journal of Physics D: Applied Physics*, vol. 56, no. 22, p. 223001, 2023. doi: 10.1088/1361-6463/acbe4c
4. R. Kakimi, M. Fujita, M. Nagai, M. Ashida, and T. Nagatsuma, "Capture of a terahertz wave in a photonic-crystal slab," *Nature Photonics*, vol. 8, no. 8, pp. 657-663, 2014. doi: 10.1038/nphoton.2014.150
5. M. A. Kats, and F. Capasso, "Optical absorbers based on strong interference in ultrathin films," *Laser & Photonics Reviews*, vol. 10, no. 5, pp. 735-749, 2016. doi: 10.1002/lpor.201600098
6. L. Ju, B. Geng, J. Horng, C. Girit, M. Martin, Z. Hao, and F. Wang, "Graphene plasmonics for tunable terahertz metamaterials," *Nature nanotechnology*, vol. 6, no. 10, pp. 630-634, 2011. doi: 10.1038/nnano.2011.146
7. B. Sensale-Rodriguez, R. Yan, M. M. Kelly, T. Fang, K. Tahy, W. S. Hwang, and H. G. Xing, "Broadband graphene terahertz modulators enabled by intraband transitions," *Nature communications*, vol. 3, no. 1, p. 780, 2012. doi: 10.1038/ncomms1787
8. P. H. Pham, W. Zhang, N. V. Quach, J. Li, W. Zhou, D. Scarmardo, and P. J. Burke, "Broadband impedance match to two-dimensional materials in the terahertz domain," *Nature Communications*, vol. 8, no. 1, p. 2233, 2017.
9. T. Zhao, P. Xie, H. Wan, T. Ding, M. Liu, J. Xie, and X. Xiao, "Ultrathin MXene assemblies approach the intrinsic absorption limit in the 0," *5-10 THz band. Nature Photonics*, vol. 17, no. 7, pp. 622-628, 2023.
10. S. Li, J. Luo, S. Anwar, S. Li, W. Lu, Z. H. Hang, and C. Wang, "Broadband perfect absorption of ultrathin conductive films with coherent illumination: Superabsorption of microwave radiation," *Physical Review B*, vol. 91, no. 22, p. 220301, 2015. doi: 10.1103/physrevb.91.220301
11. N. Luhmann, D. Høj, M. Piller, H. Kähler, M. H. Chien, R. G. West, and S. Schmid, "Ultrathin 2 nm gold as impedance-matched absorber for infrared light," *Nature communications*, vol. 11, no. 1, p. 2161, 2020.
12. D. G. Baranov, A. Krasnok, T. Shegai, A. Alù, and Y. Chong, "Coherent perfect absorbers: linear control of light with light," *Nature Reviews Materials*, vol. 2, no. 12, pp. 1-14, 2017. doi: 10.1038/natrevmats.2017.64
13. Z. Sakotic, A. Ware, M. Povinelli, and D. Wasserman, "Perfect absorption at the ultimate thickness limit in planar films," *ACS Photonics*, vol. 10, no. 12, pp. 4244-4251, 2023. doi: 10.1021/acsphotonics.3c01017
14. Z. Sakotic, A. Raju, A. Ware, F. A. Estévez H, M. Brown, Y. Magendzo Behar, and D. Wasserman, "MidInfrared Perfect Absorption with Planar and SubwavelengthPerforated Ultrathin Metal Films," *Advanced Physics Research*, vol. 3, no. 8, p. 2400012, 2024.
15. J. Horng, C. F. Chen, B. Geng, C. Girit, Y. Zhang, Z. Hao, and F. Wang, "Drude conductivity of Dirac fermions in graphene," *Physical Review B-Condensed Matter and Materials Physics*, vol. 83, no. 16, p. 165113, 2011.
16. P. A. D. Gonçalves, and N. M. Peres, "An introduction to graphene plasmonics," *World Scientific*, 2016.

and/or the editor(s) disclaim any responsibility for any injury to individuals or damage to property arising from the ideas, methods, instructions, or products mentioned in the content.